Ultramicroscopy 33 (1990) 159–166
North-Holland

ELECTRON DIFFRACTION AND LATTICE IMAGE SIMULATIONS WITH THE INCLUSION OF HOLZ REFLECTIONS

L.C. QIN and K. URBAN

Institut für Festkörperforschung, Forschungszentrum Jülich GmbH, Postfach 1913, D-5170 Jülich, Fed. Rep. of Germany

Received 20 March 1990

The formulae that can be used to calculate wave functions for transmission high-energy electron diffraction including reflections from higher-order Laue zones (HOLZs) are summarized by using the Bloch wave formulation and the multislice formulation for the dynamical electron diffraction theory, respectively. In the multislice formulation, three different algorithms of calculating phase grating functions, fraction projection algorithm (FPA), section projection algorithm (SPA) and conditional projection algorithm (CPA) are examined. Electron diffraction patterns and lattice images for the $YBa_2Cu_3O_7$ crystals are simulated and compared with Bloch wave calculations. In summary, the FPA calculations do not include HOLZ reflections; the SPA and CPA give much stronger HOLZ reflection intensities than the Bloch wave algorithm. Experimental diffraction patterns support the Bloch wave results. However, there is no detectable difference found in the simulated lattice images by using the above-mentioned computing schemes, which suggests that the HOLZ reflections only play a minor role in forming lattice images.

1. Introduction

Transmission high-energy electron diffraction from crystals can often be treated in a two-dimensional approximation by considering reflections from the zero-order Laue zone only. This is justified by the very large radius of the Ewald sphere. However, there are cases in which the third dimension becomes non-negligible, e.g., when a convergent-beam electron diffraction (CBED) pattern is used for crystallographic analyses or when the crystal unit cell dimension along the diffraction zone axis is large. In particular, this refers to alloys with large unit cells like many members of the family of tetrahedrally close-packed phases and the ceramic high T_c superconductors with c-axis lengths of from 1.2 nm for $YBa_2Cu_3O_7$ to 3.8 nm for $Bi_2Sr_2Ca_2Cu_3O_{10}$. Therefore, for the purpose of providing a reliable theoretical estimation of electron diffraction intensities and a correct interpretation of lattice images at atomic resolution, it is necessary to take into account the reflections from higher-order Laue zones (HOLZs).

When the crystal potential can be expanded as a three-dimensional Fourier series, in the Bloch wave formulation [1,2], HOLZ reflections can be included by having the corresponding Fourier components included in the dynamic matrix explicitly [3,4]. The problem can then be solved by transforming the equations into an eigensystem determined by the dynamic matrix.

In the treatment of HOLZ reflections by using the multislice formulation [5], the depth-dependence of the crystal potential within a unit cell was taken into account by using a slice thickness smaller than the crystal periodicity along the diffraction zone axis [6–8]. In practice this has led to several different algorithms for calculation of the phase grating functions that must be used in the multislice iteration procedure. These are three algorithms that can be used to prepare phase grating functions for this case. In this paper they are referred to as fraction projection algorithm (FPA), section projection algorithm (SPA) and conditional projection algorithm (CPA). Only the CPA is to give the most reliable projected potential

within a sub-slice. However, this method requires very long computing times. Therefore, in order to keep the computing time within reasonable limits, calculations have frequently been carried out by using FPA or SPA. Up to now there have been no detailed investigations to see to what extent these two approximations may be valid without introducing severe errors. Furthermore, in the multislice method a number of approximations are made whose validity needs to be tested with respect to the inclusion of HOLZ reflections in the calculations.

In this paper we first review both the Bloch wave and the multislice formulations for the dynamical electron diffraction theory with the inclusion of HOLZ reflections. In the multislice formulation we describe all three algorithms mentioned above to calculate phase grating functions in detail. As a practical example, electron diffraction patterns and lattice images from $YBa_2Cu_3O_7$ superconducting crystals along zone axis [001] are simulated by using each algorithm. The results are compared with the intensity distributions in an experimental electron diffraction pattern. We find that, although the three-dimensionality of the crystal potential has been taken into account properly in the CPA, there are still apparent discrepancies if the simulated results are compared to experimental ones. The reasons for the discrepancies found are discussed.

2. Theoretical formulations

Throughout the paper we assume that the Laue condition is satisfied, i.e. the diffraction zone axis is parallel to the surface normal of the thin crystal slab and the z-axis is chosen to be parallel to the diffraction zone axis.

2.1. Bloch wave formulation

We start from the Schrödinger equation which determines the electron wave function $\psi(\boldsymbol{r})$ within the crystal potential $V(\boldsymbol{r})$:

$$\nabla^2\psi(\boldsymbol{r}) + \frac{8\pi^2 m|e|}{h^2}\left[E + V(\boldsymbol{r})\right]\psi(\boldsymbol{r}) = 0, \qquad (1)$$

where m is the relativistic mass of the electron, E is the incident electron accelerating potential, h is Planck's constant and e is the electric charge of the electron.

Since it is periodic, we can expand the crystal potential as a Fourier series based on the reciprocal lattice:

$$V(\boldsymbol{r}) = \sum_{\boldsymbol{g}} V_{\boldsymbol{g}} \exp(2\pi i \boldsymbol{g}\cdot\boldsymbol{r}), \qquad (2)$$

where $V_{\boldsymbol{g}}$ is the gth Fourier coefficient of the potential and $\boldsymbol{g}$ is a reciprocal lattice vector.

The electron wave function within the crystal can be represented by a superposition of Bloch waves:

$$b^{(j)}(\boldsymbol{r}, \boldsymbol{k}) = \sum_{\boldsymbol{g}} C_{\boldsymbol{g}}^{(j)} \exp\left[2\pi i\left(\boldsymbol{k}^{(j)} + \boldsymbol{g}\right)\cdot\boldsymbol{r}\right], \qquad (3)$$

where $C_{\boldsymbol{g}}^{(j)}$ are the Bloch wave coefficients. By defining

$$U_{\boldsymbol{g}} = \left(2m|e|/h^2\right)V_{\boldsymbol{g}} \qquad (4)$$

and

$$K^2 = \left(2m|e|/h^2\right)(E + V_0), \qquad (5)$$

V_0 being the mean inner potential, we obtain the following by substituting eqs. (2)–(5) in eq. (1):

$$\sum_{\boldsymbol{g}}\left\{\left[K^2 - \left(\boldsymbol{k}^{(j)} + \boldsymbol{g}\right)^2\right]C_{\boldsymbol{g}}^{(j)} + \sum_{\boldsymbol{h}\neq\boldsymbol{g}} U_{\boldsymbol{g}-\boldsymbol{h}} C_{\boldsymbol{h}}^{(j)}\right\} \times \exp\left[2\pi i\left(\boldsymbol{k}^{(j)} + \boldsymbol{g}\right)\cdot\boldsymbol{r}\right] = 0. \qquad (6)$$

Eq. (6) holds for all points $\boldsymbol{r}$ in the crystal, hence the coefficient of each exponential term must be equal to zero. Thus we have the set of equations

$$\left[K^2 - \left(\boldsymbol{k}^{(j)} + \boldsymbol{g}\right)^2\right]C_{\boldsymbol{g}}^{(j)} + \sum_{\boldsymbol{h}\neq\boldsymbol{g}} U_{\boldsymbol{g}-\boldsymbol{h}} C_{\boldsymbol{h}}^{(j)} = 0. \qquad (7)$$

For each reflection $\boldsymbol{g}$ considered there is one such equation. In high-energy electron diffraction we can ignore the backscattered reflections which allows the approximation

$$K_z^2 - k_z^2 = -2K_z(k_z - K_z) = -2K_z\gamma, \qquad (8)$$

where $\gamma = k_z - K_z$ and the subscript z indicates the vector component parallel to the z-axis. Eq. (7) can then be rewritten as

$$\sum_{\boldsymbol{h}} \left[\frac{U_{\boldsymbol{g}-\boldsymbol{h}} - \left(U_0 + g^2 + 2\boldsymbol{K}\cdot\boldsymbol{g}\right)\delta_{\boldsymbol{gh}}}{2K_z(1+g_z/K_z)} \right] C_{\boldsymbol{h}} = \gamma C_{\boldsymbol{g}}, \quad (9)$$

which forms an eigensystem in which $\delta_{\boldsymbol{gh}}$ is the Kroneker symbol. All the above equations are valid for the general case of a three-dimensional crystal potential. By solving the eigenequations we may obtain the eigenvalues $\gamma^{(j)}$ (and therefore $k^{(j)}$) and eigenvectors $C_{\boldsymbol{g}}^{(j)}$.

The dynamic matrix of eq. (9) is non-Hermitian and therefore we may end up with having complex eigenvalues by using normal numerical diagonalization procedures. But we can make a non-orthogonal transformation [9], defining

$$\Gamma_{\boldsymbol{g}}^{(j)} = (1 + g_z/K_z)^{1/2} C_{\boldsymbol{g}}^{(j)}. \quad (10)$$

This yields

$$\sum_{\boldsymbol{h}} \left\{ \frac{U_{\boldsymbol{g}-\boldsymbol{h}} - \left[U_0 + g^2 + 2(\boldsymbol{K}\cdot\boldsymbol{g})\right]\delta_{\boldsymbol{gh}}}{2(K_z+g_z)^{1/2}(K_z+h_z)^{1/2}} \right\} \Gamma_{\boldsymbol{h}}^{(j)} = \gamma^{(j)} \Gamma_{\boldsymbol{g}}^{(j)}. \quad (11)$$

Now the matrix on the left-hand side is Hermitian and we obtain real eigenvalues $\gamma^{(j)}$ and unitary eigenvectors $\Gamma_{\boldsymbol{g}}^{(j)}$. By using eq. (10) we can obtain the original eigenvectors $C_{\boldsymbol{g}}^{(j)}$ as wanted. The total wave function is a linear combination of all individual Bloch waves

$$\psi(\boldsymbol{r}) = \sum_j \alpha^{(j)} \sum_{\boldsymbol{g}} C_{\boldsymbol{g}}^{(j)} \exp\left[2\pi \mathrm{i}\left(\boldsymbol{k}^{(j)} + \boldsymbol{g}\right)\cdot\boldsymbol{r}\right], \quad (12)$$

where in an ideal crystal $\alpha^{(j)}$ is the excitation amplitude of Bloch wave $b^{(j)}(\boldsymbol{r}, \boldsymbol{k})$, and

$$\alpha^{(j)} = C_0^{(j)*}. \quad (13)$$

2.2. Multislice formulation

In the multislice formulation a crystal slab is divided into many thin slices. Each slice is approximated as a phase object which modifies only the phase term of the incident electron wave. Zero potential is assumed between the neighbouring slices and the propagation of electron waves inside the gap is approximated as a Fresnel diffraction process. If $\psi_N(x, y)$ represents the two-dimensional wave function at the exit surface of the Nth slice ($z = z_N$), $q_N(x, y)$ is the phase grating function describing the phase change by the Nth slice, $p_N(x, y)$ represents the propagation function (propagator) describing the Fresnel diffraction of waves from the Nth slice (at $z = z_N$) to the $(N+1)$th slice (at $z = z_{N+1}$), then the electron wave function at the exit surface of the $(N+1)$th slice $\psi_{N+1}(x, y)$ is

$$\psi_{N+1}(x, y) = q_{N+1}(x, y)\left[\psi_N(x, y) * p_N(x, y)\right], \quad (14)$$

where $*$ denotes a convolution. The phase grating function of the $(N+1)$th slice is given by

$$q_{N+1}(x, y) = \exp\left[\mathrm{i}\sigma V_P^{(N+1)}(x, y)\,\Delta z_N\right]. \quad (15)$$

The interaction constant σ is defined as

$$\sigma = \frac{\pi}{\lambda E} \frac{2}{1 + (1+\beta^2)^{1/2}},$$

where λ is the electron wavelength and β is the relativistic factor, v/c, with v and c being the speed of the electron and that of light, respectively. The projected potential between z_N and z_{N+1} is given by

$$V_P^{(N+1)}(x, y) = \frac{1}{\Delta z_N} \int_{z_N}^{z_{N+1}} V(x, y, z)\, \mathrm{d}z, \quad (16)$$

in which $\Delta z_N = z_{N+1} - z_N$ is the thickness of the $(N+1)$th slice. And the Fresnel propagator is

$$p_N(x, y) = \frac{\mathrm{i}}{\lambda\,\Delta z_N} \exp\left[\frac{\mathrm{i}\pi}{\lambda\,\Delta z_N}\left(x^2 + y^2\right)\right]. \quad (17)$$

For simplicity, but without loss of generality, we assume in the following discussions that all slices have the same thickness of Δz and the z-axis is parallel to the c-axis of the crystal lattice. The crystal is assumed to be of orthogonal symmetry with lattice parameters a, b and c.

By substituting eq. (2) into eq. (16) we can deduce the following expression for the projected potential

$$V_P^{(N+1)}(x, y) = \frac{1}{\Delta z}\sum_{hkl} V(hkl)\frac{\sin(\pi l\,\Delta z/c)}{\pi l/c} \times \exp(2\pi i l z_{N_0}/c)\exp\left[2\pi i\left(\frac{hx}{a}+\frac{ky}{b}\right)\right], \quad (18)$$

where

$$z_{N_0} = z_N + \Delta z/2,$$

and $V(hkl)$ is the Fourier coefficient of the crystal potential at $\boldsymbol{g} = h\boldsymbol{a}^* + k\boldsymbol{b}^* + l\boldsymbol{c}^*$, in which hkl are the Miller indices of reflection (hkl) and $\boldsymbol{a}^*$, $\boldsymbol{b}^*$, $\boldsymbol{c}^*$ are the basis vectors of the reciprocal lattice. If a unit cell with length c is evenly divided into n slices, then we can have

$$V_P^{(N+1)}(x, y) = \sum_{hkl} V(hkl)\frac{\sin(\pi l/n)}{\pi l/n}\exp(2\pi i l z_{N_0}/c) \times \exp\left[2\pi i\left(\frac{hx}{a}+\frac{ky}{b}\right)\right]$$
$$= \frac{h^2}{2\pi m e V_{\text{cell}}}\sum_{hkl}\left\{\sum_{j=1}^{N_a} f_j(hkl) \times \exp\left[-2\pi i\left(\frac{hx_j}{a}+\frac{ky_j}{b}+\frac{lz_j}{c}\right)\right]\frac{\sin(\pi l/n)}{\pi l/n} \times \exp(2\pi i l z_{N_0}/c)\right\}\exp\left[2\pi i\left(\frac{hx}{a}+\frac{ky}{b}\right)\right], \quad (19)$$

where V_{cell} is the volume of the unit cell, $f_j(hkl)$ is the atomic scattering amplitude of atom type j for reflection (hkl), (x_j, y_j, z_j) are the relative coordinates of the atom in the unit cell and N_a is the total number of atoms in the unit cell. The phase grating function can be calculated by using eq. (15). When $n = 1$, i.e. the slice thickness is equal to the lattice periodicity along the diffraction zone axis, eq. (19) can be simplified using $\Delta z = c$ to

$$V_P^{(N+1)}(x, y) = \sum_{hk} V(hk0)\exp\left[2\pi i\left(\frac{hx}{a}+\frac{ky}{b}\right)\right]. \quad (20)$$

From eq. (14) we see that the multislice formulation is an iteration procedure. In this method the phase grating behaves as a scattering object which is determined by the crystal structure. It scatters the incoming electron waves from the previous slice. The propagation process, however, introduces phase changes due to the deviation from the exact Bragg condition for each beam. The function of each term can be seen more clearly if we look at formula (14) in Fourier space

$$\Phi_{N+1}(h, k) = Q_{N+1}(h, k) * [\Phi_N(h, k)\, P_N(h, k)] \quad (21)$$

and

$$P_N(h, k) = \exp\left[-i\pi\frac{(h/a)^2 + (k/b)^2}{K}\Delta z\right], \quad (22)$$

where Φ, Q, and P denote the Fourier transforms of ψ, q and p, respectively. For $n = 1$, we see from eq. (20) that all the possible interactions to be considered are those occurring between reflections on the $l = 0$ reciprocal plane. Therefore in this case HOLZ reflections are not considered. However, if $n > 1$, i.e., when the slice thickness is smaller than the crystal periodicity along the zone axis, the scattering process, which is described by $Q_{N+1}(h, k)$ in eq. (21), involves terms with $l \neq 0$. If we define a two-dimensional function $V'_{N+1}(h, k)$ as

$$V'_{N+1}(h, k) = \sum_l V(hkl)\frac{\sin \pi l/n}{\pi l/n}\exp(2\pi i l z_{N_0}/c), \quad (23)$$

then eq. (19) becomes

$$V_P^{(N+1)}(x, y) = \sum_{hk} V'_{N+1}(h, k)\exp\left[2\pi i\left(\frac{hx}{a}+\frac{ky}{b}\right)\right] \quad (24)$$

and

$$Q_{N+1}(h, k) = \mathscr{F}\left\{\exp\left[i\sigma V_P^{(N+1)}(x, y)\right] \Delta z_N\right\}.$$

Expanding the exponential function into power series we obtain

$$\begin{aligned} Q_{N+1}(h, k) &= \mathscr{F}\Big\{1 + i\sigma V_P^{(N+1)}(x, y) \\ &\quad + \frac{(i\sigma)^2}{2!}\left[V_P^{(N+1)}(x, y)\right]^2 \\ &\quad + \frac{(i\sigma)^3}{3!}\left[V_P^{(N+1)}(x, y)\right]^3 + \ldots\Big\} \\ &= \delta(h, k) + i\sigma V'_{N+1}(h, k) \\ &\quad + \frac{(i\sigma)^2}{2!} V'_{N+1}(h, k) * V'_{N+1}(h, k) \\ &\quad + \frac{(i\sigma)^3}{3!} V'_{N+1}(h, k) * V'_{N+1}(h, k) \\ &\quad * V'_{N+1}(h, k) + \ldots, \end{aligned} \tag{25}$$

where $\mathscr{F}$ represents a Fourier transform. On the right-hand side of this equation, the first term describes the forward transmission of the incident wave from the last slice, the second term describes a single scattering with scattering vector (h, k), the third term described double scattering and so forth. From this expression and taking eq. (23) into account we see that the scattering does include the HOLZ reflections with $l \neq 0$.

There are three different algorithms that have been widely used to calculate phase grating functions. They are:

(a) The fraction projection algorithm (FPA): A phase grating function calculated over the length c is evenly divided into n sub-phase grating functions.

(b) The section projection algorithm (SPA): In this algorithm, the summation in eq. (19) is carried out over those atoms only which lie within the corresponding sub-slice. The sub-slice is treated as the unit cell of an infinitely extended artificial crystal obtained by periodic stacking of these cells along the c-axis.

(c) The conditional projection algorithm (CPA): In this case, a sub-phase grating function is calculated by using eq. (19), in which the summation is done over all atoms within the unit cell of the real crystal.

In the three algorithms, the FPA always gives identical sub-phase grating functions, but SPA and CPA may give different sub-phase grating functions in general.

3. Simulations for $YBa_2Cu_3O_7$ crystals

For a demonstration we have used the $YBa_2Cu_3O_{7-x}$ crystal data in the simulations. The crystal has space group Pmmm with lattice parameters as $a = 0.382$ nm, $b = 0.389$ nm, $c = 1.168$ nm. The zone axis is chosen to be [001] and the sample thicknesses used are 46.70 nm for diffraction and 5.84 nm for lattice imaging. The accelerating voltage is 200 kV and the symmetrical Laue condition has been assumed.

3.1. Electron diffraction patterns

Fig. 1a depicts the electron diffraction pattern computed by using the Bloch wave algorithm. In total 269 beams have been included in the calculation, among which 58 beams are HOLZ reflections. The display is in a logrithmetic scale and the threshold value is 10^{-12} of the total intensity. Figs. 1b–1d give the diffraction patterns computed by using the multislice algorithm [10]. Six sub-phase gratings were used in the computations. Fig. 1b is the result with FPA phase grating and figs. 1c and 1d are the results with SPA and CPA phase gratings, respectively.

In fig. 2 an experimental electron diffraction pattern, taken from an area with thickness estimated to be around 50 nm, is given for comparison with the simulated patterns. It was taken with a JEOL 2000EX transmission electron microscope operating at 200 kV. The intensity of HOLZ reflections is extremely weak, as one can see from the negative recording films. But it vanishes on the positive prints. This result agrees well with that of

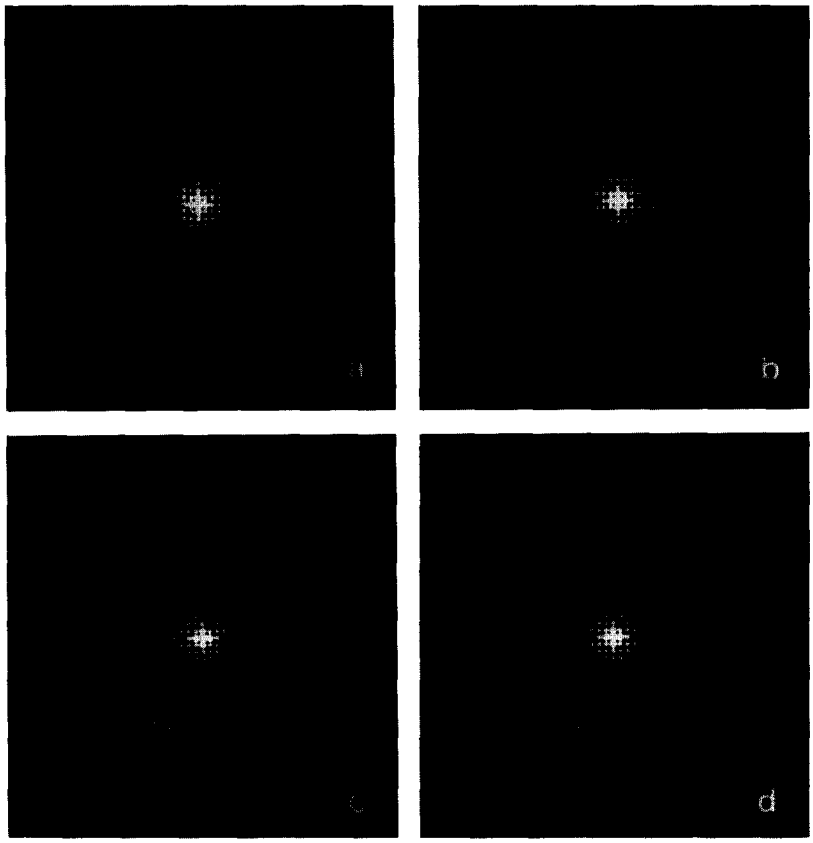

Fig. 1. Simulated 200 keV electron diffraction patterns of $YBa_2Cu_3O_{7-x}$ crystal with thickness of 46.70 nm along [001] orientation. (a) Bloch wave result; 269 beams in total including 68 HOLZ reflections. (b–d) Multislice results with 64×64 FFT algorithm and three different algorithms in calculating phase grating functions: FPA (b), SPA (c) and CPA (d).

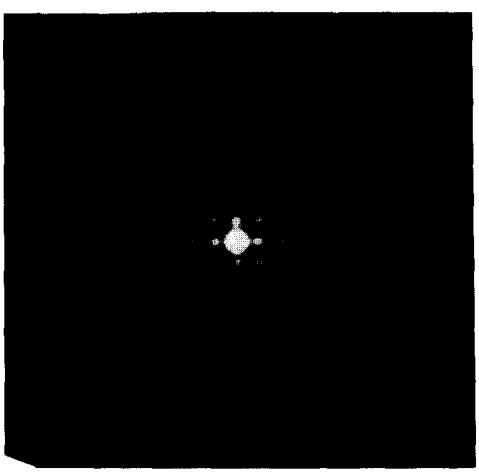

Fig. 2. An experimental diffraction pattern from $YBa_2Cu_3O_{7-x}$ crystals taken with a Jeol 2000EX electron microscope.

the Bloch wave calculations. Since FPA multislice formulae do not include HOLZ reflections, the results are likewise in agreement with the experiments. However, in disagreement with the experimental results both the SPA and CPA multislice formulae yield quite strong HOLZ reflections. So only the Bloch wave simulation is in agreement with the experiments, i.e. the HOLZ reflections are very weak.

3.2. Lattice images

By using the EMS computer code [11] we have also simulated lattice images for the same crystal, but at a smaller thickness than encountered in the experiments of lattice imaging. Fig. 3 is a halftone represention of the simulated images. The left

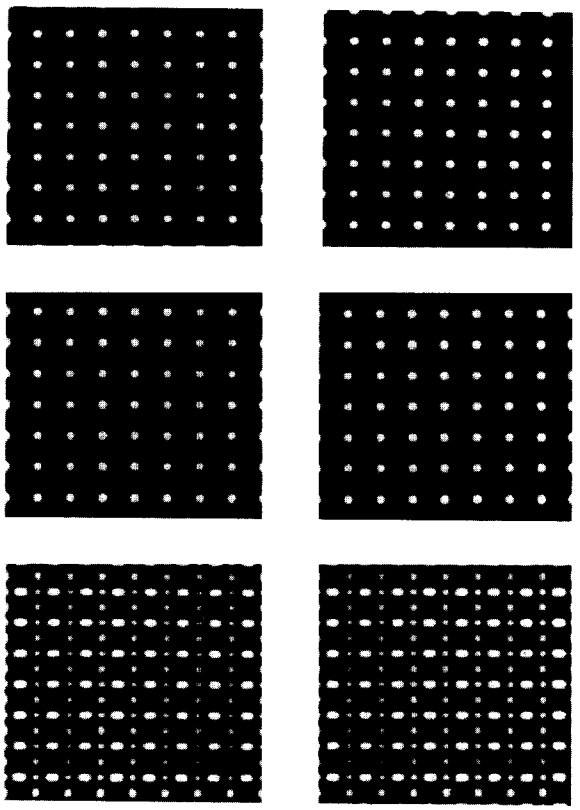

Fig. 3. Simulated lattice images of $YBa_2Cu_3O_{7-x}$ crystal at a thickness of 5.84 nm; $C_s = 1.2$ mm; objective aperture diameter = 30.0 nm^{-1}; defocus spread = 10.0 nm; semi-divergence angle = 0.5 miliradians; voltage = 200 kV. Wave function series: Bloch wave (left) and CPA multislice (right). Underfocus series: from top to bottom 67.0, 82.0 and 97.0 nm.

column gives a defocus series calculated by using the Bloch wave algorithm with 201 beams from the zero-order Laue zone. The right column shows the results of a CPA multislice computation with the same sampling parameters as described in section 3.1. All three multislice algorithms produce results identical with those of the Bloch wave calculation.

The objective aperture radius used in the simulations is 15.0 nm^{-1} corresponding to a limiting spatial resolution of about 0.6 nm (much smaller than the present information limit of modern electron microscopes) under linear imaging conditions. Therefore, although the dynamical computation of the wave function took full account of all HOLZ reflections, they were excluded by the aperture in the final image calculation.

4. Discussion

We have seen that in multislice calculations the three algorithms used for calculating phase grating functions give rise to quite different HOLZ reflection intensities. In FPA, the projected potential used in calculating the phase grating functions excludes all terms but those with $l = 0$. Therefore the contributions from HOLZ reflections are a priori not included. In SPA, it is assumed that the potential is periodic along the c-axis with the periodicity of c/n which is the thickness of each sub-slice. But the real structure has c as its periodicity along the c-axis. In general this leads to erroneous structure factors and, as a consequence, to errors in the projected potential calculated according to eq. (18). It is only the CPA that calculates the projected potential within a sub-slice correctly.

The comparison of the experimental figure with the SPA and CPA simulations revealed that there are severe discrepancies. The SPA and CPA phase gratings give much stronger intensities for HOLZ reflections while there is a good agreement with the Bloch wave calculation. This can be explained as follows: only those reflections which have small excitation errors and non-zero structure factors would occur during the scattering process. However, by looking at eq. (25) we can see that a lot of reflections that may not have small excitation errors are included in the scattering process but with quite large scattering strength (as the magnitude of the corresponding structure factor). This should account for the very large value of the intensities of those HOLZ reflections. Therefore from a general point of view, the multislice algorithm gives stronger intensities for HOLZ reflections. On the other hand, in the Bloch wave formulation, the excitation error corresponding to the relevant reflection is taken into account by the value of the diagonal terms of the dynamic matrix. Therefore the artifacts mentioned above are avoided.

Besides, the parabolic approximation to the Ewald sphere introduces some errors; in particular it does so when it is for high scattering-angle terms, such as HOLZ reflections.

Although the Bloch wave algorithm provides us with quite accurate HOLZ reflection intensities, it is not practical for many of the most interesting problems in high-resolution electron microscopy. The reasons for this are prohibitively long computation times and the rounding-off errors introduced by the diagonalization routines in computations requiring large numbers of beams, as in the image simulation of crystal defects by using the periodic continuity approximation.

As for lattice imaging, however, the contrast transfer function of an electron microscope always has an effective cut-off threshold value in spatial frequencies. This is due to the electrical instabilities of the power supply and the mechanical instabilities of the working environment. To a first approximation, they are exponential damping functions of spatial frequency. In practical experimental lattice imaging the final images will be largely determined by reflections of low spatial frequencies due to the particular shape of the contrast transfer functions. In addition, these reflections at smaller scattering angles are much stronger than the others in general. Another factor is, in most lattice imaging experiments, if not all, the objective aperture being used would have excluded any HOLZ reflections and therefore the only effect of the HOLZ reflections would then be the influence on the amplitudes of those reflections included in the aperture, which are low-order reflections. However, the influence is minor, as shown in the simulations, and therefore it is plausible to ignore the HOLZ reflections in lattice image simulations.

5. Concluding remarks

(1) When HOLZ reflection intensities are required, the Bloch wave algorithm should be used.

(2) In simulating lattice images, the existence of HOLZ reflections has only minor effects on the final image intensity, and they can usually be ignored. The three different algorithms in calculating phase grating functions do not give rise to detectable image intensity distribution. Therefore one can simply use the fraction projection algorithm (FPA) to calculate phase grating functions in order to reduce the computer time needed.

References

[1] H. Bethe, Ann. Phys. 87 (1928) 55.
[2] C.H. MacGillavry, Physica 7 (1940) 329.
[3] P.M. Jones, G.M. Rackham and J.W. Steeds, Proc. Roy. Soc. A 354 (1977) 192.
[4] A.L. Lewis, R.E. Villagrana and A.J.F. Metherell, Acta Cryst. A 34 (1978) 138.
[5] J.M. Cowley and A.F. Moodie, Acta Cryst. 10 (1957) 609.
[6] D.F. Lynch, Acta Cryst. A 27 (1971) 399.
[7] P. Goodman and A.F. Moodie, Acta Cryst. A 30 (1974) 280.
[8] R. Kilaas, M.A. O'Keefe and K.M. Krishnan, Ultramicroscopy 21 (1987) 47.
[9] P.H. Dederichs, KFA Report 107-781, 1971.
[10] D.F. Lynch and L.C. Qin, J. Appl. Cryst. 20 (1987) 442.
[11] P.S Stadelmann, Ultramicroscopy 21 (1987) 131.